A FIELD-BASED METHOD FOR ESTIMATION OF OVERLAP FOR CONVERGENT IMAGES FOR VIEW PLANNING OF BUILDINGS

A. Dashora [1]*, C. S. Utla [1], A. V. Kulkarni [2]

[1] Indian Institute of Technology Guwahati, Guwahati, India - (abd, utla176104018)@iitg.ac.in
[2] Divecha Center for Climate Change, Indian Institute of Science Banaglore, Bangalore, India - anilkulkarni@iisc.ac.in

Commission II, WG II/I

KEY WORDS: Overlap, Convergent images, Close range terrestrial photogrammetry, View planning, Building and camera geometry, Field estimation.

ABSTRACT:

Overlap between two convergent images for close-range terrestrial photogrammetry is a pre-requisite for view planning of building corners. Available tools determine overlap of images that are acquired by normal geometry at a constant distance. However, for the convergent images lengths of image footprints vary according to camera position. The paper proposes a field-based method that requires to measures only geometric dimensions of image footprints in field for assessing overlap fractions for convergent images. The paper first derives the overlap fraction of convergent images as a function of image footprints, which depend upon the camera position, object geometry, and camera FOV. Experiments are conducted in field for two building corner sites. The proposed method provides conservative estimates of overlap fractions compared to that provided by image-based methods. The errors in the overlap fractions are contributed by three sources, namely, the approximations of the proposed method, uncertainty in camera positions and alignment of camera optical axis, and placement of markers in field. Experimental results suggest that the proposed method can be used confidently in field for overlap estimation for convergent images for the view planning. Images acquired for the view planning of the two corners successfully generated 3D models.

1. INTRODUCTION

Close-range terrestrial photogrammetry (CRTP) is becoming one of the popular methods for various applications of social and commercial interests. CRTP acquires overlapping images with ease and better control using low-cost consumer grade cameras and yet delivers high resolution surface models of above ground objects situated over small areas, where data acquisition is challenged due to unavailability of GPS signals, or occluded objects and terrain surface. Recent studies highlight applications for 3D mapping and modelling of building structures, geomorphologic structure, artefacts, heritage structure, tree diameter etc (Matthews, 2008; García-Gago et al. 2014; Abbaszadeh and Rastiveisa, 2017; Mokroš et al., 2018; Baramsyah and Rich, 2019).

Above studies have mentioned that high overlap is an essential requirement for CRTP for both convergent and normal geometries between a camera and given object. For a non-topographic application, Fu et al. (2017) has found that high overlap and high resolution are necessary for the higher density and higher accuracy of photogrammetric point cloud. For most of topographic CRTP applications related to 3D model generation of non-coplanar and irregular surfaces, high overlap in range of 80-90% between two adjacent images is a pre-requisite (Haneberg, 2008; Krajnak et al., 2011; James and Robson, 2012; Westoby et al., 2012; Prieto and Ramos, 2015; Hidayat and Cahyono, 2016; Förstner and Wrobel, 2016; Micheletti et al., 2018). Similarly, for 3D models of building structures by CRTP using surface from motion (SfM) approach, a large distance between camera positions and building is selected such that each image occupies complete building information by convergent geometry (García-Gago et al., 2014). This arrangement of convergent image acquisition achieves high

overlap though, yet the arrangement compromises on high resolution. Förstner and Wrobel (2016) mention view planning exercise that considers each building corner as an individual element of a building. Further, the view planning configures camera positions at constant distance around a building corner. A block of cameras around a corner acquire images ensuring both high overlap and high resolution. Among three major goals of CRTP for 3D model generation by view planning, the 'completeness of photogrammetric information' for a 3D model can be achieved by high overlap for two non-coplanar surfaces of a corner. Therefore, if overlap is examined and evaluated for a building corner, it can work as precursor indicator and one more criterion to guarantee the 3D model generation.

Overlap can be defined as the ratio of common portion of two image footprints to footprint of any of the two images. For normal view geometry, overlap is generally measured by image-based method in field as well as in lab. Image based method overlays two images and calculates overlap using feature matching. With recent advances in algorithms of image and feature matching, sophisticated algorithms like scale invariant feature transform (SIFT) are also employed for detecting and identifying highly accurate key points and then overlap is estimated using the common key points in images (Xang et al., 2010; Li et al., 2018). However, a manual method, as described by Wolf (2018), that uses stereoscope with images is adopted with photographs.

Unlike normal images acquired by camera positions parallel to building surface, convergent geometry requires multiple camera positions on a circular path around a building corner such that camera optical axis at each camera position points to object corner. Due to this, overlap estimation for the convergent

---
* Corresponding author.
Email address: abd@iitg.ac.in

images poses some challenges. First, the convergent images should be projected with a same viewing direction for overlap estimation. However, the involved projective transformation results to large deformations for images that are acquired at angularly distant camera viewpoints. Also, for adjacent camera positions on circular path, the image footprint and consequently the image overlap vary for convergent images even at the constant radial distance from object corner. On the other hand, image-based method for overlap estimation also necessitates unique knowledge and some level of expertise for the use of sophisticated resources (sophisticated algorithms, involved techniques, and computer hardware). Considering these facts, this paper proposes and derives a field-based method for overlap measurement for the view planning of two non-coplanar surfaces of a building corner. The method requires geometric measurements and image acquisition for the surfaces of building corner in field. The paper is organized in four sections: the introduction in the first section is followed by detailed explanations of view planning and derivations of the image footprints and consequently overlap fraction in second section. Experiments and results of the proposed method is validated and discussed in section 3. In addition, the section 3 also shows the 3D models generated from the acquired images by view planning of the building corners. Conclusion is presented in section 4.

2. METHODOLOGY

2.1 Convergent Image Acquisition for Building Corner

A building corner consists of walls meeting at a specific angle. Figure 1 below showcase an image of a building corner at point O with the schematic view of camera position C acquiring the foot print OD and OE.
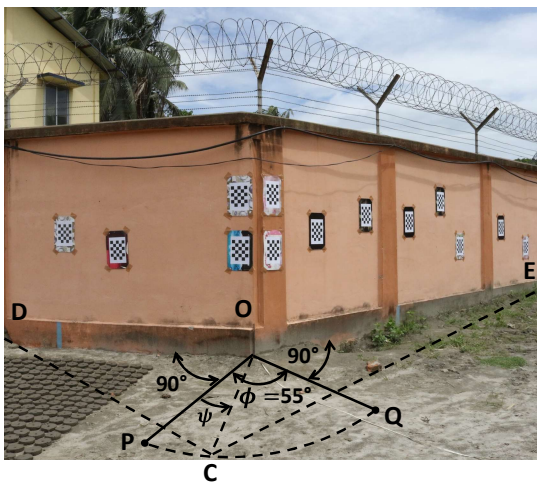

Figure 1. Footprint of convergent image and schematic details of building corner O (exterior angle of 55°, camera position C, and points P and Q on circular path, and image footprint by OD, and OE).

In above figure, lines OP and OQ are of equal lengths. Line OP and OQ are normal to left and right wall surfaces, respectively. The corner O is described by an exterior angle ϕ, which is subscribed between lines OP and OQ. Point C is a camera position measured by angle ψ from line OP on the circular path on ground defined between points P and Q. Lengths OD and OE show footprint of the image captured at point C. Figure 2

below illustrates planimetric view of a building corner O and acquisition of a convergent image at point C, which captures photogrammetric information of plane wall surfaces OU and OV.
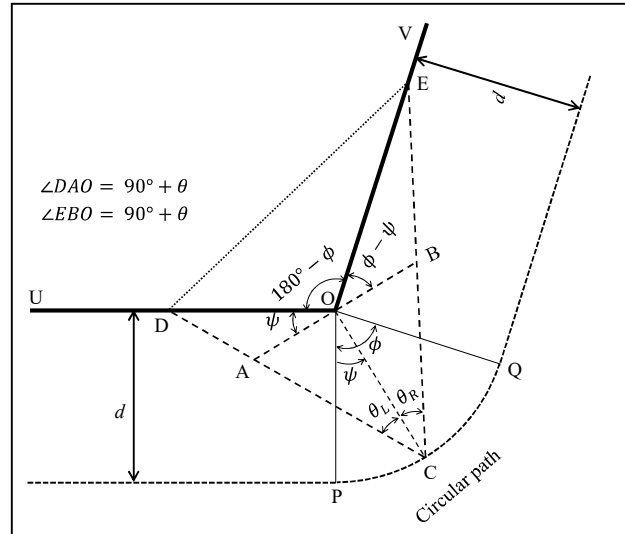

Figure 2. Image footprints of convergent image acquired on a circular path

Internal angle $\left(180° - \phi\right)$ is complementary angle of the exterior angle. Circular curve between points P and Q, marked at a distance d, indicates locus of camera positions for acquisition of convergent images at a constant distance from the corner O. Point C is the camera position on the circular path and angle ψ represents the camera position in left half of the circular path. Similarly, the line OQ is a reference line for measuring a camera position in right half of the circular path. Field of view (FOV) of a camera is generally divided in two equal parts symmetrically on either side of the optical axis. However, we are considering θ_L and θ_R for left and right parts of the FOV around the optical axis (as shown in figures in this paper).

2.2 Image Footprint of a Convergent Image

For a convergent image, such as acquired at camera position C in figure 2, the image footprint occupies object surface on both sides of point O as lengths *OD* and *OE*. From the above figure, sine rule for triangle DOA gives:

$$\frac{OD}{\sin\left(90° + \theta_L\right)} = \frac{OA}{\sin\left(90° - \theta_L - \psi\right)}$$

$$OD = \frac{d\,sin\left(\theta_L\right)}{cos\left(\theta_L + \psi\right)} \tag{1}$$

Similarly, for triangle BOE sine rule derives expression of length *OE* as:

$$OE = \frac{sin\left(\theta_R\right)}{cos\left(\theta_R + \phi - \psi\right)} \tag{2}$$

From equations 1 and 2, it is evident that the image width, expressed in two parts for a convergent image, is a function of camera FOV (θ_L, θ_R), camera position (ψ), and building corner geometry (i.e. exterior angle ϕ at a corner). For an image

captured at C, if a camera position (ψ) is located in left half of the circular path, length OD is less than length OE and vice versa. At the center point of the circular path, OD and OE are equal. Mathematical expressions of OD and OE also confirm that when exterior angle of corner (ϕ) is less than 90°, the image widths OD and OE are smaller compared to that of the exterior angle values more than 90° as camera rays intersect with the planes OU and OV at a less distance from O in former case. In forthcoming discussion, expression of overlap is derived as function of image widths OD and OE.

2.3 Overlap Fraction

Due to convergent geometry, for given combination of camera, building corner, and constant distance (d), the image width varies with the camera position (ψ). As a result, overlap fraction (η_{CC}) between the two convergent images depends up on their camera positions (ψ), FOV of camera (θ_L and θ_R), and exterior angle (ϕ) of building corner. Figure 3 shows schematic representation of the proposed method to calculate the overlap fraction of two convergent images.
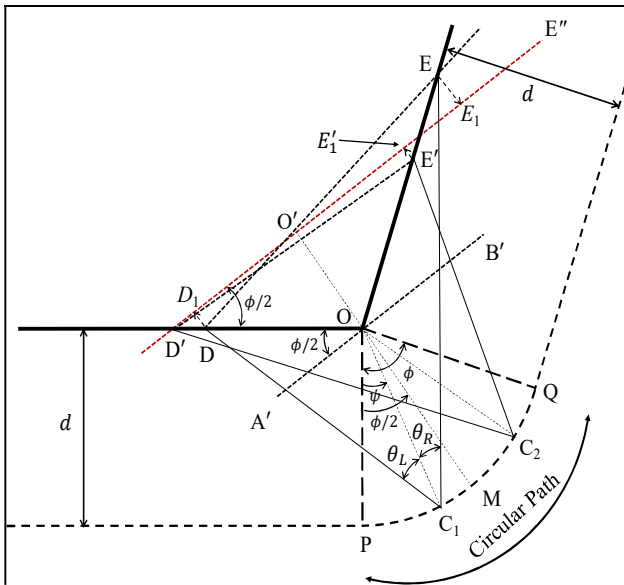

Figure 3. Figure showing overlap between convergent images acquired on circular path

According to proposed method, the image width of each convergent image is projected on a line parallel to line $A'B'$, which passes through point O and makes an angle of $\phi/2$ with both wall planes. Also, this line is divided in two equal parts by a line passing through the mid point M of the circular path. The expression of overlap for two convergent images is derived by calculating the common portions of image widths of two convergent images parallel to line $A'B'$.

The convergent image acquired at point C has image width DE (shown in figures 2 and 3). Figure 3 illustrates two camera positions, C$_1$ and C$_2$, which are located at (ψ) and ($\psi + \Delta\psi$) angles, respectively. The former and latter camera poistions acquire image footprints as DE and $D'E'$, respectively. To calculate the overlap fraction, footprints of both convergent images are projected to a line $D'E''$, which is parallel to $A'B'$

(line $D'E''$ is shown by red dotted line in figure 3). As a result, the projected points on the line $D'E''$ are: D_1 from point D, E_1 from point E, and E'_1 from point E'.

Overlap fraction, as mentioned before, is defined as the ratio of the common portion between the footprint projections of first and second images to the projected footprint of the first image on line $D'E''$. As shown in figure 3, on line $D'E''$ common length is $D_1E'_1$ and projected length of the first image is D_1E_1. Therefore, overlap fraction (η_{CC}) between the convergent images can be written as:

$$\eta_{CC} = \frac{D_1E'_1}{D_1E_1} \tag{3}$$

From the figure 3, numerator term $(D'E'_1)$ and denominator term (D_1E_1) of above expression can be written as:

$$D_1E'_1 = D'E'_1 - D'D_1 \tag{4}$$

$$D_1E_1 = D'E_1 - D'D_1 \tag{5}$$

Equations (4) and (5) modify the expression of overlap fraction as:

$$\eta_{CC} = \frac{D'E'_1 - D'D_1}{D'E_1 - D'D_1} \tag{6}$$

Equation (6) contains three variables ($D'D_1$, $D'E_1$, and $D'E'_1$). It can be observed that $D'D_1$ is the projection of the line DD' on $D'E''$. Therefore, $D'D_1$ can be expressed as:

$$D'D_1 = DD' \cos(\phi/2) \tag{7}$$

Variable $D'E_1$ is the sum of $D'O'$ and $O'E_1$, which are projections of OD' on $D'E''$ and projection of OE on $D'E''$, respectively. Mathematically, $D'E_1$ can be written as:

$$D'E_1 = D'O' + O'E_1$$

$$D'E_1 = OD' \cos(\phi/2) + OE \cos(\phi/2) \tag{8}$$

Similarly, variable $D'E'_1$ is a sum of projections of OD' and OE' on $D'E''$. Therefore,

$$D_1E'_1 = OD' \cos(\phi/2) + OE' \cos(\phi/2) \tag{9}$$

Substituting values of three variables $D'D_1$, $D'E_1$, and $D'E'_1$ from equations (7), (8), and (9) in equation (6) gives:

$$\eta_{CC} = \frac{OD' + OE' - DD'}{OD' + OE - DD'}$$

In the above expression of η_{CC}, term $OD' - DD'$ is equal to OD. Thus, η_{CC} is modified as:

$$\eta_{CC} = \frac{OD + OE'}{OD + OE} \tag{10}$$

Equation (10) provides the expresssion of overlap fraction between two convergent images. It should be noted that the left image in a pair of convergent images is consisdred as a

reference image and the variables *OD* and *OE* are appearing in the denomiator of the mathenatical expression (10). Figure 4 below expresses a simplified pictorial representation of the overlaps for the two convergent images along a straight line in field.
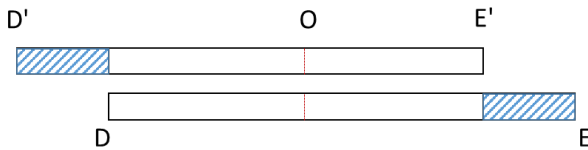

Figure 4. Pictorial representation of overlap between two convergent images

In the figure 4, for the wall corner O, *DE* and *D'E'* represent the image footprints of two convergent images on the walls. Variables involved in right hand side of the equation (10) can be measured in field for immediatiate verification of overlap fraction. On the other hand, theoritical value of overlap fraction can also be calculated by equation (10) by substituting values of *OD*, *OE* and *OE'*. From equation (2), *OE'* can be written as:

$$OE' = \frac{sin(\theta_R)}{cos(\theta_R + \phi - (\psi + \Delta\psi))} \qquad (11)$$

Substituting the values of *OD*, *OE*, and *OE'* in equation (10) gives:

$$\eta_{CC} = \frac{1 + \dfrac{cos(\theta_L + \psi)}{cos(\theta_R + \phi - (\psi + \Delta\psi))}}{1 + \dfrac{cos(\theta_L + \psi)}{cos(\theta_R + \phi - \psi)}} \qquad (12)$$

Equation (12) is a mathematical expression for calculating the overlap fraction of two convergent images which are acquired at camera positions ψ and $\psi + \Delta\psi$ on the circular path.

3. EXPERIMENTS AND RESULTS

The method for overlap estimation described above is applied for two corners of 55° and 90° exterior angles. Figures 5 and 6 show images of the two corner sites.

Figure 5. Details of the site location of 55° corner

Figure 6. Details of the site location of 90° corner

On the wall surfaces, checker boards of 37mm size (5×8 grids) are applied for validation of overlap fraction by image matching algorithms, which is an image-based method.

For each case of two corners, camera positions are decided in field such that both sides of the wall facades are visible in each image. Four camera positions (ψ) are marked on the circular path from left end of the circular path. Table 1 shows, the camera positions for the two sites.

Corner	ψ_1	ψ_2	ψ_3	ψ_4
90°	35.714°	38.50°	45°	51.50°
55°	6.875°	13.75°	27.50°	48.125°

Table 1. Camera positions (ψ) for 90° and 55° corner sites

Corresponding to above camera positions for a corner, four images are numbered as 1, 2, 3, and 4. In order to mark the camera positions on ground, two perpendiculars are drawn to both the facades of the walls for making the circular path. On these normal lines, reference points P and Q are marked on ground at shooting distance (d) from the building corner. Figure 7 shows the schematic view of the field procedure for marking a camera position for the 90° corner.
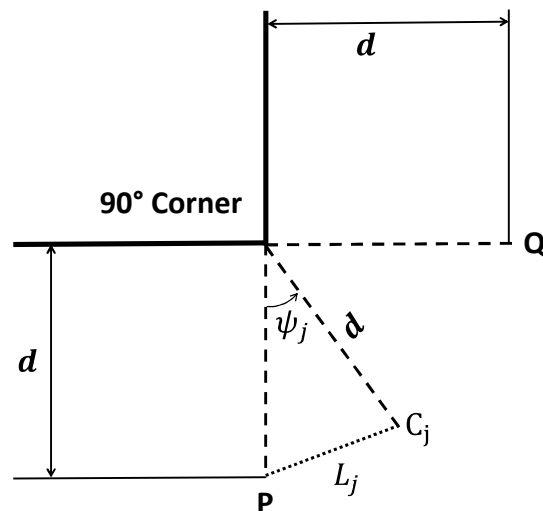

Figure 7. Schematic view of marking camera position in field for corner

A circular arc of radius d, centered at the building corner and defined between P and Q, is the circular path of camera positions. As shown in the figure 6, for a point that is located on the circular path at an angle ψ_j from line OP, chord length between points, P and C$_j$ is calculated as:

$$L_j = 2d \sin\left(\frac{\psi_j}{2}\right) \qquad (13)$$

A camera position on the circular path is marked by intersection of length d from the corner O and the length L_j from point P. Following this procedure, all camera positions are marked. To acquire the convergent images on these camera positions, Canon 7D Mark-II camera (64° FOV, 5472 x 3648 pixels) is used. The camera is mounted on a pole and aligned horizontally with the help of level and images are captured at 6m radial distance from the corner O.

Image widths on the walls are measured by marking edges of images on walls manually. Lengths of the facades covered in the images are measured in the field using a 30m tape (least count 1 cm). For both corners, sufficient lengths of planar wall surfaces are not available for image acquisition. Therefore, for demostration of overlap assesssment in field, the images are curtailed by known number of pixels and image footprints of modified images are considered for calculations. For the curtailed images, the variables θ_L and θ_R are determined and used for theoritical calculations of lengths OD and OE using equations 1 and 2, respectively. The results of OD and OE for different camera postions for the two cases are given in Table 2 and Table 3. In the tables, an image pair i-j indiates that the ith and j^{th} images are acquired from their respective camera positions from the left edge of the circular path. Moreover, the ith image is reference image for calculations of overlap fractions by equations (10) and (12). Furthermore, length OE of the jth image or latter image of the image pair should be considered as OE', which can also be calculated by equation (11). For example, the image pair 1-2, describes that the 1st and 2nd images are acquired from camera positions ψ_1 and ψ_2, respectively, and the 1st image is the reference image for overlap fraction calculations. For the calculations of variable $\Delta\psi$, one should select $\psi_1 < \psi_2$. Theoretical estimate of the overlap fraction can be calculated in multiple steps using equations (1), (2), (10), and (11). On the other hand, equation (12) provides the overlap estimate in one step. In tables 2 and 3, estimated values by formula and measured values in field for two lengths (OD and OE) are shown for the two corner sites.

Image Pair	Camera FOV		Estimated values		Measured values in field	
	θ_L	θ_R	OD	OE	OD	OE
1-3	32	21.754	8.38	9.22	8.66	9.09
			14.13	5.63	14.47	5.83
2-3	32	23.626	9.53	9.37	9.83	9.09
			14.13	6.60	14.47	7.2
3-4	32	27.626	14.13	9.32	14.47	9.09
			28.09	6.87	27.63	7.2
1-4	32	21.754	8.38	9.22	8.66	9.09
			28.09	4.48	27.63	4.81

Table 2. Theoritical Values and Field Measurements for 90° Corner (FOV values and lengths are in degrees and meter units)

Image Pair	Camera FOV		Estimated values		Measured values in field	
	θ_L	θ_R	OD	OE	OD	OE
1-3	24.702	25.333	2.94	9.02	3.15	9.22
			3.20	6.46	3.31	6.80
2-3	14.269	29.544	1.68	8.99	1.76	9.22
			1.98	5.44	2.08	5.60
3-4	10.222	32.000	1.84	6.26	1.97	5.89
			2.91	4.08	3.15	4.05
1-4	24.702	25.333	1.62	9.02	1.76	9.22
			2.04	4.25	2.04	4.45

Table 3. Theoritical Values and Field measurements for 55° Corner (FOV values and lengths are in degrees and meter units)

Using estiamtes and field observations of image widths (variables OD and OE), the overlap is estimated by the proposed method. For validating the results of the proposed object-based method, an image-based method demonstrated by Xing et al (2010) is adopted. Accordingly, an open source image-based soft copy method developed by Garg 2018 is used. The algorithm performs image matching and detects common matches. Coordinates of common matches are determined and overlap is calculated by conventional approach, which is used for stereo images, i.e. overlap is estimated as if two convergent images are stereo images. For 90° and 55° corners, Table 4 and Table 5 present the overlap calculations obtained by measurements in field (η_F) and by the analytical equations (η_S) of the proposed method. These values are validated against the overlap obtained by the image-based method (η_I).

Image Pair	η_S	η_F	η_I
1-3	79.64	81.63	85.02
2-3	85.34	90.01	92.92
3-4	89.58	91.98	93.45
1-4	73.09	75.89	78.76

Table 4. Percentage Overlap Values for 90° Corner

Image pair	η_S	η_F	η_I
1-2	78.62	80.44	84.81
2-3	66.68	67.02	73.38
3-4	73.08	76.59	79.13
1-3	55.20	56.55	61.77

Table 5. Percentage Overlap Values for 55° Corner

Results in Tables 2, 3, 4 and 5 confirm that the image footprint size and overlap fractions for convergent images vary according to camera positions. In Tables 2 and 3, the difference of the

theoretical values and field measurements for image footprints are in range of 28-46 cm and 0-37 cm for 90° and 55° corners, respectively. The errors are biased towards the right side of the images. Moreover, higher errors can be observed for larger image footprints. On the other hand, these error values are equivalent to 30-110 average pixels for the given image characteristics. For a camera of 5472 pixels, the maximum amount of the errors in variables OD or OE is approximately 5% of total pixels in half portion of an image. Sources of errors are contributed by centering of camera positions, orientation of camera axes (tilt of camera frame, tilts of optical axis in normal and vertical direction), and marking of image edges as well as length measurements for OD and OE variables in field. In the field experiments, marking of camera positions by the intersection process has also contributed to errors for camera positions, which are in addition to errors for centering the camera in field at a location. Amongst all sources of errors, maximum errors are contributed by optical axis orientation and camera position as the former error cannot be controlled in object surface and latter one originates from marking procedure adopted. While performing experiments in field, raw estimates confirm that camera position may be incorrect in range of 2-10cm and optical axis may show deviation in range of 0.25-1.5°. These values of errors should be accounted for analysis while estimating the error budget for this method.

Results in Tables 4 and 5 express that overlap fractions calculated by field measurements and mathematical expressions are in close agreement. On the other hand, the results of overlap fraction by the proposed method are conservative or under-estimate of the overlap fraction calculated by conventional approach of image-based method. Convergent images acquired for two corners are used for 3D model generation by pix4D software. Figures 8 and 9 showcase the generated 3D models. These figures validate the results of view planning performed for the two corners.

Figure 8: 3D mesh model of 55° corner

Figure 9: 3D mesh model of 90° corner

3D model of two corner contains high resolution details. Details in the two figures are limited to corners. For 3D model of 90° corner in figure 9, homogenous surface or uniform texture lacks the features and thus the model contains voids in right wall. In addition, geometry of 90° corner allows less overlap compared to 55° corner. Consequently, smaller lengths for the building surfaces is obtained in 3D model for the 90° corner.

Authors have also conducted experiments for both corners with higher number of images (staring from 3 to 10 convergent images on the circular path). Experiments confirm that higher number of convergent images increases the overlap fraction between adjacent images and consequently spatial extent of 3D model of the corner increases. In addition, higher values of point cloud density of the 3D model are achieved.

4. CONCLUSION

This paper proposes an object-based approach for overlap estimation in field for convergent images for view planning of building corners. The paper considers the convergent geometry of image acquisition for a building corner and derives mathematical expressions for estimating the overlap fraction both in laboratory and field. The expressions for overlap calculations in field are simple as well as elegant for use with an electronic calculator or developing a monograph for a given camera and building corner geometry. For two corner sites of exterior angles 55° and 90°, experiments are conducted in field. Image footprints and overlap fractions are measured and results are validated. The overlap fractions for convergent images should not be assumed constant as the overlap fractions for convergent images vary according to camera positions. The experiments, theoretical calculations, and validation show close agreement among overlap fraction values for both corner sites. Reliable results suggest that the field-based method is an alternate to the image-based methods in lab for convergent images. Moreover, the method can be implemented in field with

minimum expertise because one needs to measure only geometric dimensions of convergent images (or footprints) for a building corner in field. Furthermore, generated 3D model of the two corners sites also confirm that field-based measurements of overlap fraction demonstrated in this paper can be used for view planning exercise for building corners consisting of two non-coplanar surfaces. Moreover, repeating this exercise for each building corner can create seamless 3D model of the building by convergent images. Authors also envision that the similar methods can be developed for validation of overlaps in field for various CRTP applications for irregular surface formed by multiple non-coplanar surfaces.

REFERENCES

Abbaszadeh, S. and Rastiveisa, H., 2017. A comparison of close-range photogrammetry using a nonprofessional camera with field surveying for volume estimation. *The International Archives of the Photogrammetry, Remote Sensing and Spatial Information Sciences*, *Tehran's Joint ISPRS Conferences of GI Research, SMPR and EOEC 2017*, 7–10 October 2017, Tehran, Iran.

Baramsyah, H. and Rich, L., 2019. Applicability assessments of close-range photogrammetry for rock slope face 3D modelling. *Aceh International Journal of Science and Technology,* 8(3), 144-151. doi: 10.13170/aijst.8.3.14650

Förstner, W. and Wrobel, B., 2016. *Photogrammetric Computer Vision*. Springer Nature.

Fu, X., Peng, C., Li, Z., Liu, S., Tan M. and Song J., 2017. The application of multi-baseline digital close-range photogrammetry in three-dimensional imaging and measurement of dental casts. PLoS ONE, 12(6), e0178858. URL: https://doi.org/10.1371/journal.pone.0178858

García-Gago, J., González-Aguilera, D., Gómez-Lahoz, J., José-Alonso, S. and Ignacio, J., 2014. A photogrammetric and computer vision-based approach for automated 3D architectural modeling and its typological analysis. *Remote Sensing*, 6(6), 5671-5691.

Garg, A., 2018. Feature Matching.
URL: https://github.com/ayushgarg31/Feature-Matching.

Haneberg, W. C., 2008. Using close range terrestrial digital photogrammetry for 3-D rock slope modeling and discontinuity mapping in the United States. *Bulletin of Engineering Geology and the Environment,* 67(4), 457-469.

Hidayat, H. and Cahyono, A. B., 2016. Combined aerial and terrestrial images for complete 3D documentation of Singosari temple based on Structure from Motion algorithm. *2nd International Conference of Indonesian Society for Remote Sensing (ICOIRS) 2016, IOP Conference Series: Earth and Environmental Science*, 47(1), 012004.

James, M. R. and Robson, S., 2012. Straightforward reconstruction of 3D surfaces and topography with a camera: Accuracy and geoscience application. *Journal of Geophysical Research*, 117(F03017), 17 pages.

Li, J., Huang, D. and Yang P., 2018. Inspection method of images' overlap of UAV photogrammetry based on features matching. *MATEC Web of Conferences 173, SMIMA 2018*. URL: https://doi.org/10.1051/matecconf/2018173 (last accessed March 15, 2022)

Matthews, N. A., 2008. Aerial and close-range photogrammetric technology: Providing resource documentation, interpretation, and preservation. *Technical Note 428. U.S. Department of the Interior, Bureau of Land Management*, National Operations Center, Denver, USA, 42 pages. URL: https://www.blm.gov/sites/blm.gov/files/documents/files/Library_BLMTechnicalNote428_0.pdf (last accessed March 13, 2022)

Mokroš, M., Liang, X., Surový, P., Valent, P., Cernava, J., Chudý, F., Tunák, D., Salon, Š. and Merganic, J., 2018. Evaluation of close-range photogrammetry image collection methods for estimating tree diameters. *ISPRS International Journal of Geo-Information*, 7, 93, 13 pages. doi:10.3390/ijgi7030093

Prieto, G. R. and Ramos, A. P., (2015). Modeling and accuracy assessment for 3D-virtual reconstruction in cultural heritage using low-cost photogrammetry: Surveying of the "Santa María Azogue" church's front. *The International Archives of Photogrammetry, Remote Sensing and Spatial Information Sciences,* 40(5), 263.

Westoby, M.J., Brasington, J., Glasser, N.F., Hambrey, M.J., and Reynolds, J.M., 2012. 'Structure-from-Motion' photogrammetry: A low-cost, effective tool for geoscience applications. *Geomorphology*, 15 pages. doi: http://dx.doi.org/10.1016/j.geomorph.2012.08.021

Wolf, P.R., 2018. *Elements of photogrammetry.* McGraw-Hill Education, New York.

Xing, C., Wang, J. and Xu, Y., 2010. Overlap analysis of the images from unmanned aerial vehicles. *IEEE International Conference on Electrical and Control Engineering*, 1459-1462.